Chinese Journal of Chemical Engineering 25 (2017) 924–930

Contents lists available at ScienceDirect

Chinese Journal of Chemical Engineering

journal homepage: www.elsevier.com/locate/CJChE

Separation Science and Engineering

Synthesis of clay-supported nanoscale zero-valent iron using green tea extract for the removal of phosphorus from aqueous solutions

Akbar Soliemanzadeh *, Majid Fekri

Department of Soil Science, College of Agriculture, Shahid Bahonar University of Kerman, Kerman, Iran

ARTICLE INFO

Article history:
Received 17 May 2016
Received in revised form 26 December 2016
Accepted 27 December 2016
Available online 13 January 2017

Keywords:
Green tea
Nano zero-valent iron
Natural bentonite
Phosphorus
Sorption

ABSTRACT

This study addresses the synthesis of nanoscale zero-valent iron (nZVI) in the presence of natural bentonite (B-nZVI) using green tea extract. The natural bentonite and B-nZVI were then applied for the removal of phosphorus from aqueous solutions at various concentrations, pH levels and contact time. The desorption of phosphorus (P) from adsorbents was done immediately after sorption at the maximum initial concentration using the successive dilution method. The characterization of FTIR, SEM, and XRD indicated that nZVI was successfully loaded to the surface of natural bentonite. The sorption of phosphorus on B-nZVI was observed to be pH-dependent, with maximum phosphorus removal occurring at the pH range of 2 to 5. The results demonstrate that the maximum sorption capacities of natural bentonite and B-nZVI were 4.61 and 27.63 $mg \cdot g^{-1}$, respectively. Langmuir, Freundlich, and Redlich–Peterson models properly described the sorption isotherm data. For either adsorbent, desorption isotherms did not coincide with their corresponding sorption isotherms, suggesting the occurrence of irreversibility and hysteresis. The average percentages of retained phosphorus released from natural bentonite and B-nZVI were 80% and 9%, respectively. The results indicated that sorption kinetics was best described by the pseudo-second-order model. The present study suggests that B-nZVI could be used as a suitable adsorbent for the removal of phosphorus from aqueous solutions.

1. Introduction

Although phosphorus is an essential element to all forms of life on Earth, its excessive amounts lead to eutrophication in natural environments such as reservoirs, lakes, and coastal areas [1]. Eutrophication is the over enrichment of natural waters with mineral nutrients, particularly phosphorus and nitrogen [2]. Phosphorus is introduced to natural waters by several exogenous sources such as fertilizers, industry, household detergents, and weathering rock [2]. Xu *et al.* [3] reported that eutrophication threshold of total phosphorus (TP) for freshwaters was from 0.02 to 0.10 $mg \cdot L^{-1}$. Therefore, it is necessary to isolate phosphorus from natural waters to avoid possible hazardous exposure.

In recent years, because of the growing importance of nanotechnologies, nanoscale zero-valent iron (nZVI) has been investigated and used in the removal of phosphorus from aqueous systems due to its large active surface area and high phosphorus sorption capacities [4–6]. Chemical and physical methods have been used to synthesize of nZVI, including top-down and bottom-up methods [7]. However, the limitations of these methods are that they are usually expensive, require specific and costly equipment, consume high amount of energy, produce flammable hydrogen gas, and use toxic chemical materials such as sodium borohydride ($NaBH_4$), organic solvents, and stabilizing and dispersing agents [7,8]. Therefore, the development of nonhazardous, bio-based, low-cost, simple, and eco-friendly synthesized methods for nZVI is needed. In this approach, the green synthesis of nZVI using extracts of plant products such as green tea leaves [9–11], eucalyptus leaves [12,13], and mint leaves [14], has been developed. The plant extracts are used as reducing and capping agents due to their antioxidant contents such as polyphenols, reducing sugars, nitrogenous bases, and amino acids [15,16].

In this work, a non-toxic biodegradable, and water soluble polyphenol extracted from commercial green tea was selected as the reducing and stabilizing agent for nZVI production. Previous studies have reported that green synthesized nZVI was non-toxic and used for the removal of arsenic [17,18], chromium [19], and nitrate [13] from aqueous solutions.

Clay minerals such as zeolite, sepiolite, and bentonite are basically hydrous aluminum silicates having small particle sizes (<2 μm). Bentonite is a member of smectite family and has unique characteristics such as large specific surface area, high cation exchange capacity (CEC), low-cost, and wide-spread availability, which makes it suitable for hosting nZVI. In addition, previous studies reported that the synthesis of nZVI in the presence of clay minerals (montmorillonite and bentonite) decreases their aggregation by partial dispersion/adsorption onto the clay surface [18,20].

The main objectives of the present work were to investigate (1) the synthesis of green nZVI using commercial green tea leaves in the presence of natural bentonite, (2) characterization of natural bentonite and B-nZVI by infrared spectroscopy (FTIR), scanning electron microscope

* Corresponding author.
E-mail address: asoliemanzadeh@yahoo.com (A. Soliemanzadeh).

http://dx.doi.org/10.1016/j.cjche.2016.12.006
1004-9541/

(SEM), and X-ray diffraction (XRD), and (3) evaluation of the sorption characteristics of phosphorus on natural bentonite and B-nZVI.

2. Materials and Methods

2.1. Materials

All the chemicals used in the present study, including ferrous sulfate heptahydrate ($FeSO_4 \cdot 7H_2O$), sodium hydroxide (NaOH), potassium dihydrogen phosphate (KH_2PO_4), sulfuric acid (H_2SO_4), ammonium molybdate $(NH_4)_6Mo_7O_{24}$), antimony potassium tartrate ($K(SbO) \cdot C_4H_4O_6 \cdot 0.5H_2O$), and ascorbic acid were of analytical grade (chemical purity > 99%, Merck). The commercial leaves of green tea were used as sources of polyphenols. Natural bentonite used in the present study was obtained from Yazd Province, Iran. Based on an XRF analysis, the chemical composition of the natural bentonite sample (%) was: SiO_2, 66.37; Al_2O_3, 13.24; Fe_2O_3, 2.04; MgO, 2.37; CaO, 1.79; and Na_2O, 1.69.

2.2. Preparation of B-nZVI

For the synthesis of B-nZVI, 4 g of natural bentonite was added to 50 ml of 0.1 $mol \cdot L^{-1}$ $FeSO_4 \cdot 7H_2O$ and the mixture was mixed for 30 min using a magnetic stirrer. Meanwhile, green tea extract was prepared by adding 20 g of leaves of green tea to 1 L of distilled water, and heating at 80 °C for 1 h. Then, the extract was filtered and added drop-wise to 0.1 $mol \cdot L^{-1}$ of $FeSO_4 \cdot 7H_2O$ and natural bentonite mixture at the volume ratio of 1:1 at room temperature with constant stirring. The immediate color change of the mixture to black indicated the formation of iron nanoparticles. The suspension was centrifuged and washed with ethylene to remove the residual ferrous sulfate heptahydrate. The wet paste was then left to dry overnight.

2.3. Characterization of natural bentonite and B-nZVI

Surface functional groups of natural bentonite, P sorption on natural bentonite, B-nZVI, and P sorption on B-nZVI were examined using KBr pressed disk technique by FT-IR spectroscopy (Model: Bruker, TENSOR 27, Germany). The spectra obtained in the range of 500–4000 cm^{-1} were analyzed.

A KYKY EM-3200 scanning electron microscope (SEM) was used for surface morphological and structural studies of natural bentonite and B-nZVI.

The XRD patterns of natural bentonite and B-nZVI were recorded on B-nZVI were recorded on a Philips X'pert Pro MPD model X-ray diffractometer (Netherlands) using CuK_α radiation as the X-ray source.

2.4. Batch experiment

The stock solution containing 1000 $mg \cdot L^{-1}$ phosphorus was prepared by dissolving 4.39 g of KH_2PO_4 in distilled water, and the desired solutions were prepared by dilution of the stock solution.

The phosphorus sorption isotherms were conducted based on batch equilibrium technique. 0.05 g of absorbent samples (natural bentonite or B-nZVI) was added into conical centrifuge tubes with 10 ml of aqueous solution containing various amounts of phosphorus concentrations (10, 50, 100, 200, 300, 400 and 500 mg) in 0.01 $mol \cdot L^{-1}$ NaCl in triplicate. Then, the suspensions were shaken at room temperature and at the constant agitation rate of 300 $r \cdot min^{-1}$ using a shaker for 24 h. At the end of equilibrium, the suspensions were centrifuged and the equilibrium phosphorus concentrations were measured using the ascorbic acid method [21] and UV–vis spectrophotometer at the wavelength of 880 nm.

In pH studies (adsorbent dose = 5 $g \cdot L^{-1}$; phosphorus initial concentration = 100 and 500 $mg \cdot L^{-1}$), the pH value of reaction mixture was adjusted to the range of 2–10 with 0.1 $mol \cdot L^{-1}$ NaOH or 0.1 $mol \cdot L^{-1}$ HCl, and a pH-meter (Jenway, United Kingdom) was used to determine the pH value. The amount of phosphorus adsorbed per gram adsorbent q ($mg \cdot g^{-1}$) and removal efficiency (%) of phosphorus can be determined according to the following equations:

$$q = \frac{(C_i - C_e)V}{W} \tag{1}$$

$$\text{Removal} = \frac{(C_i - C_e)}{C_i} \times 100\% \tag{2}$$

where C_i and C_e ($mg \cdot L^{-1}$) are phosphorus initial and equilibrium concentrations, respectively; V (L) is the volume of the solution; W (g) is the dose of natural bentonite or B-nZVI.

The effect of contact times in the range of 0–1440 min was investigated with adsorbent doses of 5 $g \cdot L^{-1}$ and phosphorus initial concentration of 500 $mg \cdot L^{-1}$. The sorption amount at time of t (min), q_t ($mg \cdot g^{-1}$), was determined according to the following equation:

$$q_t = \frac{(C_i - C_t)V}{W} \tag{3}$$

where C_i and C_t ($mg \cdot L^{-1}$) are phosphorus concentrations at first and the time of t, respectively.

2.5. Phosphorus desorption experiment

Desorption experiments were carried out using the method described by [22]. Desorption of phosphorus from natural bentonite and B-nZVI was done immediately after sorption at the 500 $mg \cdot L^{-1}$ initial concentration using the successive dilution method. After shaking the phosphorus–sorbent suspensions at room temperature for 24 h, the supernatants were separated by centrifugation. Then, 10 ml of the supernatant was removed to measure phosphorus concentration, and replaced with 10 ml of 0.01 $mol \cdot L^{-1}$ NaCl. This desorption cycle was repeated 6 and 9 times for natural bentonite and B-nZVI, respectively, and desorption isotherms were prepared by plotting the phosphorus remained on the adsorbents after each desorption cycle *versus* the corresponding equilibrium phosphorus concentrations in the solution.

3. Results and Discussion

3.1. Characterization

The characterization of natural bentonite (a), P sorption on bentonite (b), B-nZVI (c) and P sorption on B-nZVI (d) by FTIR is shown in Fig. 1. The IR spectrum of natural bentonite demonstrates that hydrogen-bonded of water H–O–H and H–O–H deformation was at 3427.75 and 1640.96 cm^{-1}, respectively. However, the spectral band of 3630.03 cm^{-1} has been identified to stretching of octahedral O–H groups that attached to Al^{+3} or Mg^{+2}. The Si–O and Si–O–Si groups of the tetrahedral sheet stretching were at 795.04 and 1040.02 cm^{-1}, respectively. The band at 635.33 cm^{-1} is assigned to the out-of-plane vibrations of coupled Al–O and Si–O. Similar functional groups were also reported by other studies [23]. When comparing Fig. 1a and c, the shift of 1640.96 cm^{-1} band to 1683.31 and the presence of a new band at 1384 cm^{-1} show the loading of nZVI particles to natural bentonite. These results are confirmed by other researchers [18]. The results of Fig. 1d show that the absorption band at 1384 cm^{-1} became insignificant, and the intensity of the peak at 1683.31 cm^{-1} was decreased. Probably, the sorption of phosphorus on the B-nZVI resulted in the weakening of the band at 1384 cm^{-1} and decreased the intensity of the peak at 1683.31 cm^{-1}.

The SEM images of natural bentonite and B-nZVI are presented in Fig. 2, indicating that the nZVI loaded to the natural bentonite is generally spherical in shape and has an average diameter of 40–60 nm.

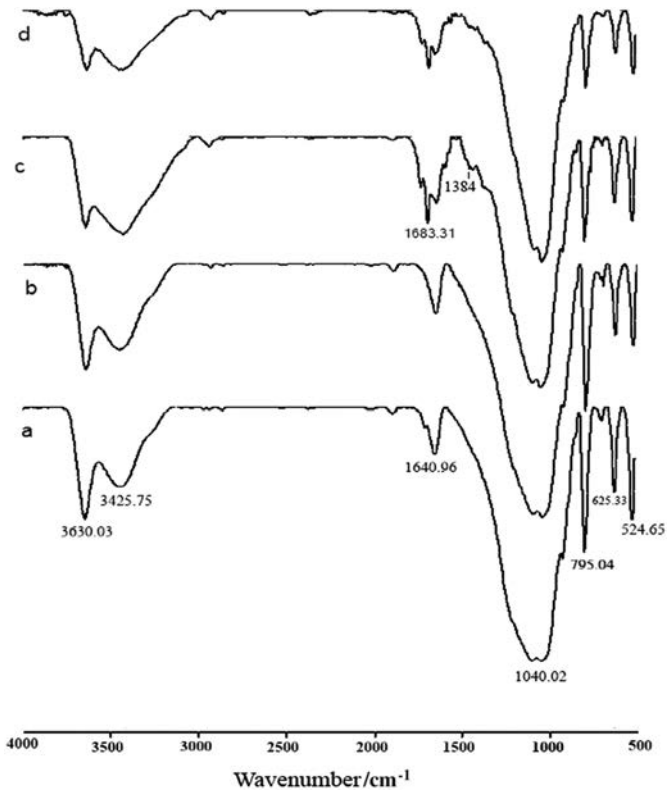

Fig. 1. FTIR spectra of natural bentonite (a), P sorption on natural bentonite (b), B-nZVI (c), and P sorption on B-nZVI (d).

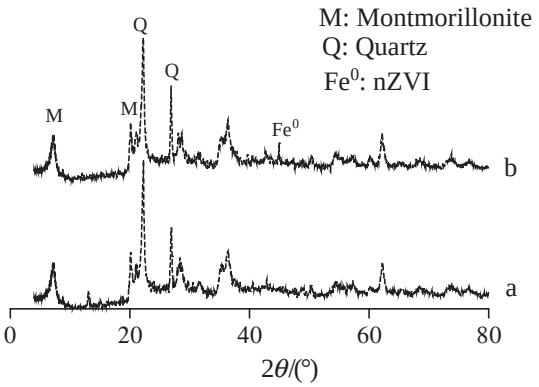

Fig. 3. XRD patterns of natural bentonite (a), B-nZVI (b).

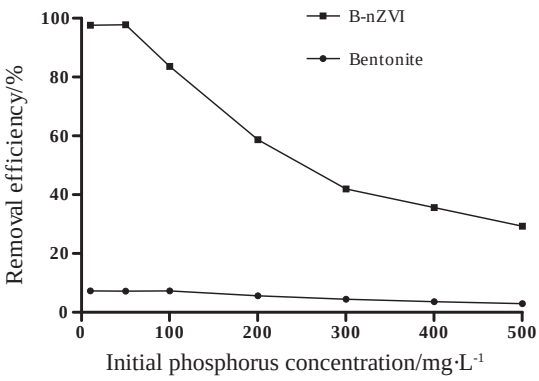

Fig. 4. Effect of initial phosphorus concentration on the removal of phosphorus by natural bentonite and B-nZVI.

The XRD patterns of natural bentonite (a) and B-nZVI (b) are shown in Fig. 3. The XRD pattern of B-nZVI shows the main diffraction peaks at the 2θ value of 44.9° which are related to the dispersion of nZVI to the surface of natural bentonite. As can be seen from Fig. 3b, diffraction peaks corresponding to the structure of natural bentonite existed in the XRD pattern of the B-nZVI, which shows that the bentonite structure is not destroyed after reaction with nZVI [24,25].

3.2. Effect of initial concentration on the removal of phosphorus

The results of present study showed that the increase in phosphorus initial concentration led to a decrease in the removal efficiency of phosphorus (Fig. 4). The removal efficiency of B-nZVI was higher than that of natural bentonite. The maximum percentages of phosphorus removal by B-nZVI (97.78%) and natural bentonite (7.29%) were observed at 50 and 10 mg·L^{-1} of phosphorus initial concentration, respectively. As initial concentrations of phosphorus increased from 50 to 500 mg·L^{-1}, removal efficiency by B-nZVI decreased from 97.78% to 29.25%, while removal by natural bentonite decreased from 7.18% to 2.91%.

It is a well-known fact that the removal efficiency of a sorption phenomenon depends upon the ratio of the number of adsorbate moieties to the available active sites of adsorbent. However, this ratio is related to the adsorbent surface coverage (number of active sites occupied/number of active sites available) that increases with the increase in the number of adsorbate moieties per unit volume of solution at a fixed dose of adsorbent [26]. By increasing the initial concentration, the available active sites of adsorbent become saturated by phosphorus

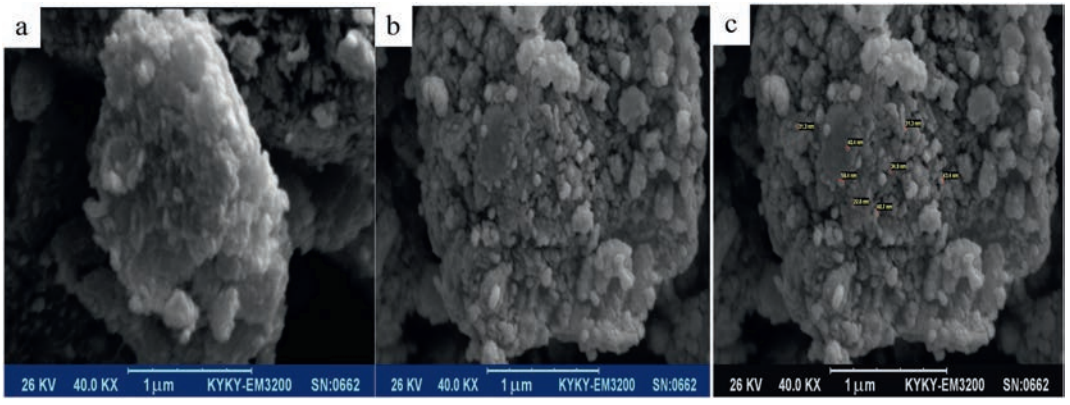

Fig. 2. SEM images of natural bentonite (a) and B-nZVI (b and c).

ion which finally results an increase in this ratio and decrease in removal efficiency.

3.3. Effect of pH on the removal of phosphorus

Experiments were conducted at different ranges of pH including 2, 4, 5, 6, 8, and 10 (Fig. 5). The optimum pH for the removal of phosphorus by B-nZVI ranged from 2 to 5 for both 100 and 500 mg·L^{-1} of phosphorus. With an increase of pH from 5 to 8, the sorption capacity decreased from 16.72 to 8.25 and 29.25 to 20.45 mg·g^{-1} for 100 and 500 mg·L^{-1} of phosphorus initial concentration, respectively. The results of the present study showed that the B-nZVI sorption capacity was relatively constant at an acidic solution pH (2–5), whereas B-nZVI sorption capacity decreased sharply as the solution pH approached a highly alkaline condition.

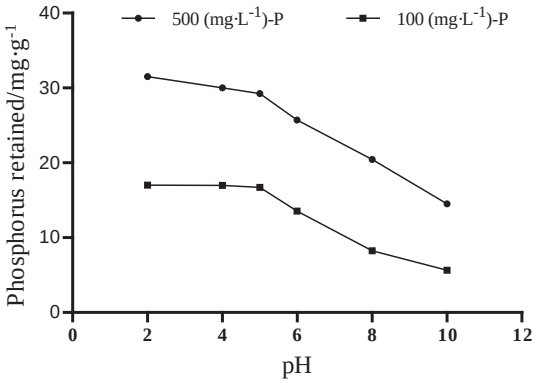

Fig. 5. Effect of pH on phosphorus removal by B-nZVI.

The maximum phosphorus removal by B-nZVI was observed at the pH range of 2 to 5, at which interval the dominant phosphorus species is the monovalent $H_2PO_4^{-1}$ ion. This was due to the change in dominant aqueous phosphorus species as a function of pH. At the lowest range of pH, more H^+ ions become available on the surface of B-nZVI and the surface becomes more positively charged, leading to the higher adsorption of phosphorus. At the height range of pH, the activity of OH^- in the solution, which competed with the phosphorus species, becomes higher [27]. However, Yan et al. [28] reported that the optimal pH for phosphorus adsorption on Al-bentonite and Fe–Al-bentonite ranges from 3 to 5. This agreed with the report of other researchers on the effect of pH on phosphorus sorption which indicates a lower pH being favorable to phosphorus sorption [6,29–31].

3.4. Sorption isotherms

Sorption isotherms are useful tools for understanding the sorption phenomenon by different adsorbents. In the present study, Freundlich (Eq. (4)), Langmuir (Eq. (5)), and Redlich–Peterson (Eq. (6)) isotherm models were used to describe the sorption capacity of natural bentonite and B-nZVI for phosphorus.

$$q = K_{\text{sorb}} C_e^{\frac{1}{n_{\text{sorb}}}} \tag{4}$$

$$q = \frac{Q_{\max} K_L C_e}{1 + K_L C_e} \tag{5}$$

$$q = \frac{A\, C_e}{1 + B C_e^g} \tag{6}$$

Where C_e and q are the equilibrium concentration of phosphorus in the aqueous solution and the amount of phosphorus ions sorbed to the adsorbent, respectively; K_{sorb} and $1/n_{\text{sorb}}$ are Freundlich constants related to sorption capacity and sorption intensity, respectively; K_L and $Q_{\max}$ are Langmuir constants related to the affinity of binding sites and maximum sorption capacity, respectively; and A, B, and g are Redlich–Peterson constants related to sorption capacity, affinity of binding sites and sorption intensity, respectively.

The equilibrium isotherm model parameters are shown in Table 1. For Langmuir isotherm parameters, the values of $Q_{\max}$ were determined to be 4.61 and 27.63 mg·g^{-1} for natural bentonite and B-nZVI, respectively. These values indicate that the loading of nZVI to natural bentonite increased the phosphorus sorption capacity by 6 times. In addition, the bonding energy coefficient value (K_l) of B-nZVI is greater than that of natural bentonite, which is related to the specifically sorbed phosphorus at high energy.

Table 1
Sorption isotherm parameters of phosphorus onto natural bentonite and B-nZVI

Types	Natural bentonite	B-nZVI
Langmuir		
$Q_{\max}$	4.61	27.63
K_l	0.004	0.13
R^2	0.94	0.91
SE	0.30	3.29
Freundlich		
	Sorption	
K_{sorb}	0.09	8.35
$1/n_{\text{sorb}}$	0.57	0.22
R^2	0.91	0.96
SE	0.37	2.13
	Desorption	
K_{desob}	0.53	26.43
$1/n_{\text{desorb}}$	0.27	0.01
R^2	0.88	0.86
SE	0.28	0.31
Redlich–Peterson		
A	0.01	30.27
B	0.004	2.62
g	2.05	0.84
R^2	0.95	0.97
SE	0.26	1.75

The Langmuir constant K_L can be treated as an empirical equilibrium constant and used in the evaluation of the standard free energy of adsorption using the following equation [17,32]:

$$\Delta G^0 = -RT \ln K_L \tag{7}$$

where ΔG^0 is the Gibb's standard free energy, R is the gas constant (= 8.314 J·mol^{-1}·K^{-1}), T is the temperature (K), and K_L is the Langmuir constant (L·mol^{-1}). The ΔG^0 values for B-nZVI and natural bentonite were −20.57 and −11.94 kJ·mol^{-1}, respectively. These negative values show that the phosphorus sorption phenomenon was spontaneous.

The phosphorus sorption data of natural bentonite and B-nZVI best fitted to the Freundlich model. The value of $1/n_{\text{sorb}}$ in Freundlich isotherm was lower than 1, suggesting that this model is nonlinear, which is a usual behavior for adsorbents with fixed and limited sorption capacities. For the Freundlich isotherm, the K_{sorb} values for natural bentonite and B-nZVI were 0.09 and 8.31, respectively. The value of K_{sorb} increased with nZVI loading to natural bentonite surface similar to the Langmuir ($Q_{\max}$ and K_L) and Redlich–Peterson (A and B) isotherm constants indicating the increase in capacity of phosphorus sorption on the sorbents. Comparison of R^2 values obtained from models shows that the Redlich–Peterson model gave a better fit result than other models.

3.5. Desorption experiment

Comparison of phosphorus sorption–desorption patterns on/from natural bentonite and B-nZVI is shown in Fig. 6. Desorption isotherms did not fit with their corresponding sorption isotherms, and sorption–desorption hysteresis occurred, meaning that irreversibility happened in phosphorus sorption in the time-scale of this experiments.

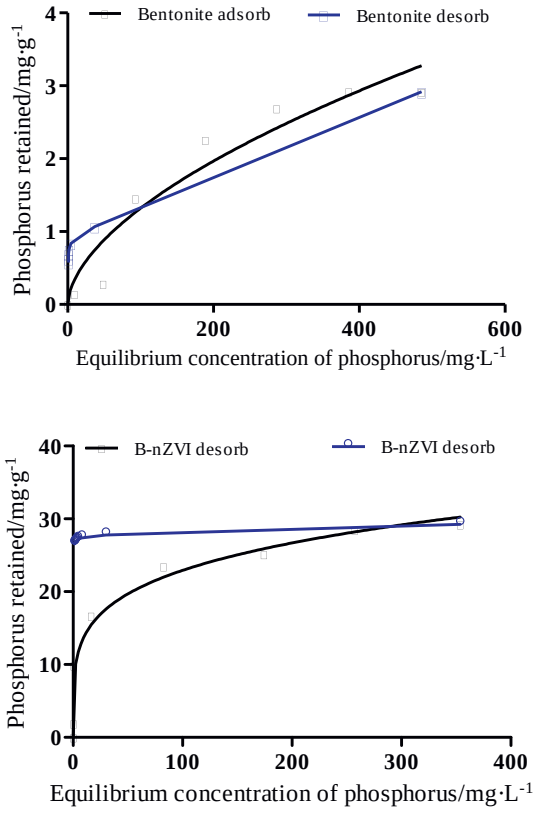

Fig. 6. Phosphorus sorption–desorption for the natural bentonite and B-nZVI.

Fig. 6 shows that the sorption of phosphorus on natural bentonite was more reversible than that of B-nZVI. The average percentages of the retained phosphorus released from natural bentonite (after six successive desorption steps) and B-nZVI (after nine successive desorption steps), were 80% and 9%, respectively. This can be due to the stronger interaction between phosphorus anions and the nZVI that were loaded to the natural bentonite surface. It may be concluded that the less irreversibility of phosphorus sorption by B-nZVI was due to the inner-sphere binding and covalent bonds of phosphorus to the nZVI surface [33]. However, Moharami and Jalali [29] reported that maximum phosphorus desorbed from Al_2O_3, Fe_3O_4 and TiO_2 nanoparticles was 6.5%, 5.9% and 2.8%, respectively.

As can be seen from Fig. 6, after 1 step of desorption, 63% of the retained phosphorus was released from the natural bentonite that is equal to 1.85 $mg \cdot g^{-1}$. This suggests that outer-sphere complexation is the dominant mechanism of sorption reaction between phosphorus and bentonite, and that phosphorus sorption was likely reversible and less specific. These results are in agreement with those obtained by Moharami and Jalali [34] which observed that 41.9% of phosphorus was released from bentonite.

Similar sorption isotherm, the desorption isotherm was calculated using Freundlich equations;

$$q = K_{\text{desorb}} C_e^{\frac{1}{n_{\text{desorb}}}} \tag{8}$$

where K_{desorb} and $1/n_{\text{desorb}}$ are Freundlich bounding constants for the desorption coefficient.

Various studies showed that Freundlich model was the most popular one to explain metals sorption–desorption phenomenon by different adsorbents [35–37]. For each sorbent, the K value (Freundlich constant) calculated from sorption isotherms was lower than that determined from desorption isotherms. Also, this parameter was remarkably higher for B-nZVI than the one obtained from natural bentonite, showing the occurrence of a positive hysteresis and a remarkably lower desorption of sorbed phosphorus from the B-nZVI than from natural bentonite. Dhillon and Brar [38] and Jalali and Naderi Peikam [39] have also reported hysteresis in phosphorus sorption–desorption phenomenon in soils.

3.6. Sorption kinetics

The pseudo-first-order (Eq. (9)), pseudo-second-order (Eq. (10)), and intra-particle diffusion (Eq. (11)) models were applied to describe the sorption kinetics of phosphorus to natural bentonite and B-nZVI (Fig. 7).

$$q_t = q_{\max}\left(1 - e^{-k_1 t}\right) \tag{9}$$

$$q_t = \frac{k_2 q_{\max}^2 t}{1 + k_2 q_{\max} t} \tag{10}$$

$$q_t = k_p t^{1/2} + C \tag{11}$$

Where q_t and $q_{\max}$ (sorption capacity) are the amounts of phosphorus sorbed at time the of t and equilibrium, respectively; k_1 and k_2 are pseudo-first-order rate constant and pseudo-second-order rate constant, respectively; and k_p and C are the intra-particle diffusion rate constant and intercept at the ordinate, respectively.

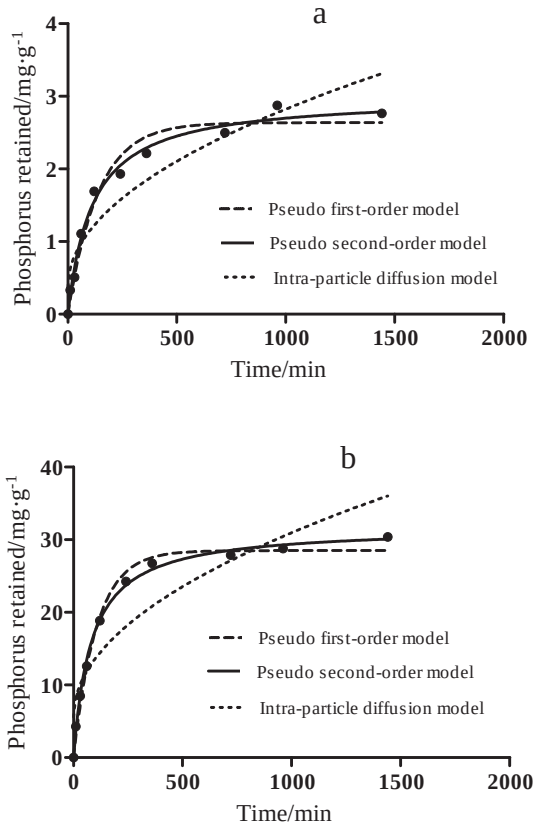

Fig. 7. Kinetic model analyses for natural bentonite (a) and B-nZVI (b).

Table 2
Kinetic model parameters for natural bentonite and B-nZVI

Sorbents	Pseudo first-order model			Pseudo second-order model				Intra-particle diffusion		
	q_{max}/mg·g^{-1}	k_1/min^{-1}	r^2	q_{max}/mg·g^{-1}	k_2/mg·g^{-1}·min^{-1}	h/mg·g^{-1}·min^{-1}	r^2	k_p/mg·g^{-1}·min$^{-0.5}$	C/mg·g^{-1}	r^2
Bentonite	2.63	0.007	0.91	3.00	0.002	0.02	0.97	0.07	0.37	0.87
B-nZVI	28.51	0.009	0.93	31.79	0.0003	0.30	0.99	0.80	5.59	0.83

The correlation coefficient (r^2) of pseudo-second-order equation is higher than those of pseudo-first-order and intra-particle diffusion (Table 2), suggesting that the chemisorption process could be a rate-limiting step [27–29,40,41]. In pseudo-second-order model parameters, the q_{max} value for B-nZVI was higher than that obtained from natural bentonite, indicating that loading nZVI to natural bentonite surface remarkably increased phosphorus sorption capacity. However, the values of k_2 decreased with loading nZVI to natural bentonite surface, demonstrating that the time required to reach equilibrium has increased.

The initial sorption constant (h) at $t \to 0$ was calculated using the following Eq. (12) [40,42]:

$$h = k_2 q_{max}^2 \tag{12}$$

The value of h obtained from B-nZVI was higher than the one obtained from natural bentonite, indicating that loading of nZVI to natural bentonite increased sorption at an initial phase of the sorption process.

According to the intra-particle diffusion model (Fig. 8), a plot of q_t *versus* $t^{1/2}$ presented multi-linearity, with an initial linear phase followed by an intermediate linear phase and a plateau, showing that two or more steps govern the sorption phenomenon.

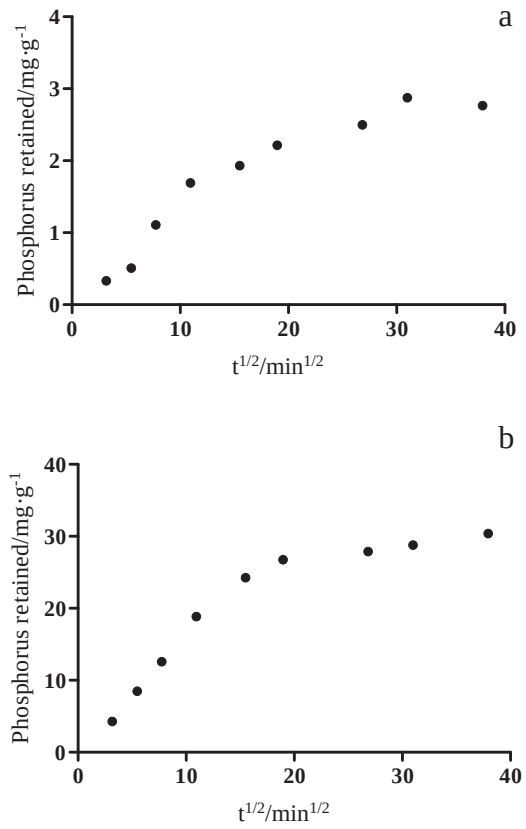

Fig. 8. Intra-particle diffusion plots for phosphorus sorption onto natural bentonite (a) and B-nZVI (b).

The initial sharper phase is attributed to the external surface or the instantaneous sorption, and the second linear phase is attributed to the gradual sorption stage where pore diffusion is rate-controlling [27,42–44]. The third phase is attributed to the final sorption equilibrium stage where intra-particle diffusion started to slow down due to the following reasons: a) small pores for diffusion, b) high electrostatic repulsion of the natural bentonite and B-nZVI surface, and c) low concentration of phosphorus in the solution [27,45]. Intra-particle diffusion is the sole rate-limiting step if the plot of q_t *versus* $t^{1/2}$ passes through the origin. In the present study, the plot of natural bentonite and B-nZVI did not pass through the origin, indicating that three processes control the sorption rate, but only one is rate-limiting in any particular time range [42].

The values of k_p and C were determined from the slope of the second linear phase (Fig. 8, Table 2). In the present study, the values of k_p and C increased from 0.07 to 0.80 and from 0.37 to 5.59, respectively, as the nZVI loading to the surface of natural bentonite. A higher C value shows a greater effect of boundary layer, suggesting that the internal mass transfer is favored over external mass transfer [43,44].

4. Conclusions

In this study, the natural bentonite and B-nZVI were applied to remove phosphorus from aqueous solutions. For both adsorbents, increasing the phosphorus initial concentration decreased removal efficiency. The sorption of phosphorus on B-nZVI was observed to be pH-dependent, with maximum phosphorus removal occurring at the pH range of 2 to 5. The sorption capacity of B-nZVI was higher than that of natural bentonite. Langmuir, Freundlich, and Redlich–Peterson models properly described the sorption isotherm data. The sorption–desorption of phosphorus by natural bentonite and B-nZVI showed hysteresis. The results indicated that sorption of phosphorus was more reversible on natural bentonite than on B-nZVI. The pseudo-second-order model fitted well to the kinetic data, suggesting that the chemisorption process could be a rate-limiting step. The present study suggests that B-nZVI can be used as a suitable adsorbent for the removal of phosphorus from aqueous solutions.

References

[1] M.A. Tabatabai, D.L. Sparks, L. Al-Amoodi, W. Dick, Chemical Processes in Soils, Soil Science Society of America Inc., 2005
[2] M. Kagami, Y. Hirose, H. Ogura, Phosphorus and nitrogen limitation of phytoplankton growth in eutrophic Lake Inba, Japan, *Limnology* 14 (2013) 51–58.
[3] H. Xu, H.W. Paerl, B. Qin, G. Zhu, G. Gao, Nitrogen and phosphorus inputs control phytoplankton growth in eutrophic Lake Taihu, China, *Limnol. Oceanogr.* 55 (2010) 420.
[4] H. Liu, T. Chen, X. Zou, Q. Xie, C. Qing, D. Chen, R.L. Frost, Removal of phosphorus using NZVI derived from reducing natural goethite, *Chem. Eng. J.* 234 (2013) 80–87.
[5] F. Liu, J. Yang, J. Zuo, D. Ma, L. Gan, B. Xie, P. Wang, B. Yang, Graphene-supported nanoscale zero-valent iron: Removal of phosphorus from aqueous solution and mechanistic study, *J. Environ. Sci.* 26 (2014) 1751–1762.
[6] T. Almeelbi, A. Bezbaruah, Aqueous phosphate removal using nanoscale zero-valent iron, *J. Nanopart. Res.* 14 (2012) 1–14.
[7] S. Machado, S. Pinto, J. Grosso, H. Nouws, J.T. Albergaria, C. Delerue-Matos, Green production of zero-valent iron nanoparticles using tree leaf extracts, *Sci. Total Environ.* 445 (2013) 1–8.
[8] L. Huang, X. Weng, Z. Chen, M. Megharaj, R. Naidu, Synthesis of iron-based nanoparticles using oolong tea extract for the degradation of malachite green, *Spectrochim. Acta A Mol. Biomol. Spectrosc.* 117 (2014) 801–804.
[9] M.N. Nadagouda, A.B. Castle, R.C. Murdock, S.M. Hussain, R.S. Varma, In vitro biocompatibility of nanoscale zerovalent iron particles (NZVI) synthesized using tea polyphenols, *Green Chem.* 12 (2010) 114–122.

[10] L. Huang, F. Luo, Z. Chen, M. Megharaj, R. Naidu, Green synthesized conditions impacting on the reactivity of Fe NPs for the degradation of malachite green, *Spectrochim. Acta A Mol. Biomol. Spectrosc.* 137 (2015) 154–159.
[11] C. Mystrioti, N. Papassiopi, A. Xenidis, D. Dermatas, M. Chrysochoou, Column study for the evaluation of the transport properties of polyphenol-coated nanoiron, *J. Hazard. Mater.* 281 (2015) 64–69.
[12] Z. Wang, Iron complex nanoparticles synthesized by eucalyptus leaves, *ACS Sustain. Chem. Eng.* 1 (2013) 1551–1554.
[13] T. Wang, X. Jin, Z. Chen, M. Megharaj, R. Naidu, Green synthesis of Fe nanoparticles using eucalyptus leaf extracts for treatment of eutrophic wastewater, *Sci. Total Environ.* 466 (2014) 210–213.
[14] K.S. Prasad, P. Gandhi, K. Selvaraj, Synthesis of green nano-iron particles (GnIP) and their application in adsorptive removal of As(III) and As(V) from aqueous solution, *Appl. Surf. Sci.* 317 (2014) 1052–1059.
[15] V.V. Makarov, S.S. Makarova, A.J. Love, O.V. Sinitsyna, A.O. Dudnik, I.V. Yaminsky, M.E. Taliansky, N.O. Kalinina, Biosynthesis of stable iron oxide nanoparticles in aqueous extracts of *Hordeum vulgare* and *Rumex acetosa* plants, *Langmuir* 30 (2014) 5982–5988.
[16] S. Quideau, D. Deffieux, C. Douat-Casassus, L. Pouységu, Plant polyphenols: chemical properties, biological activities, and synthesis, *Angew. Chem. Int. Ed.* 50 (2011) 586–621.
[17] N. Horzum, M.M. Demir, M. Nairat, T. Shahwan, Chitosan fiber-supported zero-valent iron nanoparticles as a novel sorbent for sequestration of inorganic arsenic, *RSC Adv.* 3 (2013) 7828–7837.
[18] P.K. Tandon, R.C. Shukla, S.B. Singh, Removal of arsenic (III) from water with clay-supported zerovalent iron nanoparticles synthesized with the help of tea liquor, *Ind. Eng. Chem. Res.* 52 (2013) 10052–10058.
[19] M. Chrysochoou, C.P. Johnston, G. Dahal, A comparative evaluation of hexavalent chromium treatment in contaminated soil by calcium polysulfide and green-tea nanoscale zero-valent iron, *J. Hazard. Mater.* 201 (2012) 33–42.
[20] R. Abbassi, A.K. Yadav, N. Kumar, S. Huang, P.R. Jaffe, Modeling and optimization of dye removal using “green” clay supported iron nano-particles, *Ecol. Eng.* 61 (2013) 366–370.
[21] E.W. Rice, L. Bridgewater, A.P.H. Association, Standard Methods for the Examination of Water and Wastewater, American Public Health Association Washington, DC2012.
[22] S. Bakhtiary, M. Shirvani, H. Shariatmadari, Adsorption–desorption behavior of 2, 4-D on NCP-modified bentonite and zeolite: Implications for slow-release herbicide formulations, *Chemosphere* 90 (2013) 699–705.
[23] K. Bukka, J.D. Miller, J. Shabtai, FTIR study of deuterated montmorillonites; Structural features relevant to pillared clay stability, *Clay Clay Miner.* 40 (1992) 92–102.
[24] L. Chen, Y. Huang, L. Huang, B. Liu, G. Wang, S. Yu, Characterization of Co(II) removal from aqueous solution using bentonite/iron oxide magnetic composites, *J. Radioanal. Nucl. Chem.* 290 (2011) 675–684.
[25] A. Soliemanzadeh, M. Fekri, The application of green tea extract to prepare bentonite-supported nanoscale zero-valent iron and its performance on removal of Cr(VI): Effect of relative parameters and soil experiments, *Microporous Mesoporous Mater* 239 (2017) 60–69.
[26] P. Mondal, C.B. Majumder, B. Mohanty, Effects of adsorbent dose, its particle size and initial arsenic concentration on the removal of arsenic, iron and manganese from simulated ground water by Fe^{3+} impregnated activated carbon, *J. Hazard. Mater.* 150 (2008) 695–702.
[27] Z. Wang, E. Nie, J. Li, M. Yang, Y. Zhao, X. Luo, Z. Zheng, Equilibrium and kinetics of adsorption of phosphate onto iron-doped activated carbon, *Environ. Sci. Pollut. Res.* 19 (2012) 2908–2917.
[28] L.G. Yan, Y.Y. Xu, H.Q. Yu, X.D. Xin, Q. Wei, B. Du, Adsorption of phosphate from aqueous solution by hydroxy-aluminum, hydroxy-iron and hydroxy-iron–aluminum pillared bentonites, *J. Hazard. Mater.* 179 (2010) 244–250.
[29] S. Moharami, M. Jalali, Effect of TiO_2, Al_2O_3, and Fe_3O_4 nanoparticles on phosphorus removal from aqueous solution, *Environ. Prog. Sustain. Energy* 33 (2014) 1209–1219.
[30] D. Wu, Y. Shen, A. Ding, M. Qiu, Q. Yang, S. Zheng, Phosphate removal from aqueous solutions by nanoscale zero-valent iron, *Environ. Technol.* 34 (2013) 2663–2669.
[31] A. Soliemanzadeh, M. Fekri, S. Bakhtiary, M.H. Mehrizi, Biosynthesis of iron nanoparticles and their application in removing phosphorus from aqueous solutions, *Chem. Ecol.* 32 (2016) 286–300.
[32] Y. Liu, Some consideration on the Langmuir isotherm equation, *Colloids Surf. A Physicochem. Eng. Asp.* 274 (2006) 34–36.
[33] Z. Wen, Y. Zhang, C. Dai, Removal of phosphate from aqueous solution using nanoscale zerovalent iron (nZVI), *Colloids Surf. A Physicochem. Eng. Asp.* 457 (2014) 433–440.
[34] S. Moharami, M. Jalali, Removal of phosphorus from aqueous solution by Iranian natural adsorbents, *Chem. Eng. J.* 223 (2013) 328–339.
[35] M. Kragović, A. Daković, M. Marković, J. Krstić, G.D. Gatta, N. Rotiroti, Characterization of lead sorption by the natural and Fe(III)-modified zeolite, *Appl. Surf. Sci.* 283 (2013) 764–774.
[36] M. Hamidpour, M. Kalbasi, M. Afyuni, H. Shariatmadari, P.E. Holm, H.C.B. Hansen, Sorption hysteresis of Cd(II) and Pb(II) on natural zeolite and bentonite, *J. Hazard. Mater.* 181 (2010) 686–691.
[37] Y. Aşçi, Ü. Açikel, Y.S. Açikel, Equilibrium, hysteresis and kinetics of cadmium desorption from sodium-feldspar using rhamnolipid biosurfactant, *Environ. Technol.* 33 (2012) 1857–1868.
[38] N. Dhillon, B. Brar, Influence of long-term use of fertilizers and farmyard manure on the adsorption–desorption behaviour and bioavailability of phosphorus in soils, *Nutr. Cycl. Agroecosyst.* 75 (2006) 67–78.
[39] M. Jalali, E.N. Peikam, Phosphorus sorption–desorption behaviour of river bed sediments in the Abshineh river, Hamedan, Iran, related to their composition, *Environ. Monit. Assess.* 185 (2013) 537–552.
[40] S.Y. Yoon, C.G. Lee, J.A. Park, J.H. Kim, S.B. Kim, S.H. Lee, J.W. Choi, Kinetic, equilibrium and thermodynamic studies for phosphate adsorption to magnetic iron oxide nanoparticles, *Chem. Eng. J.* 236 (2014) 341–347.
[41] S. Benyoucef, M. Amrani, Adsorption of phosphate ions onto low cost Aleppo pine adsorbent, *Desalination* 275 (2011) 231–236.
[42] H.K. Boparai, M. Joseph, D.M. O'Carroll, Kinetics and thermodynamics of cadmium ion removal by adsorption onto nano-zerovalent iron particles, *J. Hazard. Mater.* 186 (2011) 458–465.
[43] W. Liu, J. Zhang, C. Zhang, Y. Wang, Y. Li, Adsorptive removal of Cr(VI) by Fe-modified activated carbon prepared from *Trapa natans* husk, *Chem. Eng. J.* 162 (2010) 677–684.
[44] R.K. Bharali, K.G. Bhattacharyya, Biosorption of fluoride on Neem (*Azadirachta indica*) leaf powder, *J. Environ. Chem. Eng.* (2015).
[45] H. Koyuncu, A.R. Kul, An investigation of Cu (II) adsorption by native and activated bentonite: Kinetic, equilibrium and thermodynamic study, *J. Environ. Chem. Eng.* 2 (2014) 1722–1730.